DOI: 10.1002/ejic.200800966

Morphogenesis of CuI Nanocrystals by a TSA-Assisted Photochemical Route: Synthesis, Optical Properties, and Growth Mechanism

Baocheng Zhang,[a] Anjian Xie,[a,b] Yuhua Shen,*[a,b] Liangbao Yang,[a] Yiping Huang,[a] and Jingjing Lu[a]

Keywords: Copper / CuI / Nanocrystals / Crystal growth / Crystal engineering / Photochemistry / Optical properties

Synthesis of nanosized CuI crystals has become more and more important due to their wide range of applications. However, it is usually difficult to control the morphology and size of CuI crystals because of the preferential growth of the (111) face. In this study, single-crystalline γ-CuI nanocrystals with diamond and platelet morphologies have been successfully synthesised by utilising UV-irradiated 12-tungstosilicate (TSA) as a reducing agent for the reduction of Cu^{2+} under ambient conditions. A possible growth mechanism has been proposed and this suggests that the formation of diamond-shaped CuI nanocrystals is in accordance with homogeneous nucleation theory and the formation of CuI platelets is due to reaction-controlled growth with (111) facets as the basal planes. Both diamond-shaped and platelet-shaped CuI nanocrystals have a strong emission band at 365 nm which is different from the previous reports and a high electrical conductivity, indicating their promising applications in optical and electronic nanodevices.

Introduction

Since the physical and chemical properties of materials have an affinitive relationship with their size and shape, much research attention has been focused on finding ways to conveniently control the size and morphology of nanostructures during synthesis.[1] Among the different nanometre-scale particles, the preparation and characterisation of semiconductor particles represents an important field as a consequence of the potential utilisation of the latter in optics, electrics and catalysis etc.[2] Over the past two decades, excitons and the self-trapping of holes in I–VII semiconductor materials have been studied.[3] Cuprous iodide (CuI), as a kind of p-type high bandgap material, has attracted more and more attention in recent years due to its wide-ranging applications. For example, CuI thin films have the potential for application in different kinds of electronic devices.[4] CuI also serves as a catalyst in a variety of organic reactions.[5] A variety of synthetic methods for CuI crystals have been used, such as the hydrothermal method,[6,7] the decomplexation method,[8] in situ etching[9,10] and the PEG-assisted method[11] etc. However, most of the products obtained with the above methods are sheets or microsized particles. Until now, reports on synthesising nanosized CuI with a uniform morphology are very few. Because the growth behaviour of CuI crystals is difficult to control, it is still a great challenge to prepare CuI nanocrystals with a uniform morphology.

We report herein, for the first time, a room temperature preparation and growth history of single-crystalline diamond-shaped and platelet-shaped γ-CuI nanocrystals by using Keggin ions as shape control and redox agents.

Over the last century studies on Keggin ions, an important family of inorganic cluster compounds, have been mainly focused on catalytic and photochemical properties.[12–15] In recent years, Keggin ions have been exploited as functional templates for the controlled synthesis of inorganic nanomaterials due to their unique structures, reversible redox properties, greater stability and low toxicity. The synthesis of the noble metal nanoparticles with Keggin ions as photocatalysts and stabilisers has been pioneered by E. Papaconstantinou et al.[16] They employed Keggin ions as photocatalysts for reduction and recovery of copper.[17] M. Sastry and coworkers employed $[PW_{12}O_{40}]^{3-}$ ions as UV-switchable reducing agents to synthesise Au core-Ag shell nanoparticles.[18] They have also used $[PW_{12}O_{40}]^{3-}$ as templates for in situ growth of Ag nanoparticles and Pd nanoparticles.[19,20] Very recently, we reported hydrothermal treatment to form Se microwire networks,[21] UV irradiation for the synthesis of Se@Ag and Se@Au nanoparticles[22] and the morphology controlled synthesis of a silver nanocomplex in TSA solution.[23]

[a] School of Chemistry and Chemical Engineering, Anhui University,
Hefei 230039, P. R. China
Fax: +86-551-5108702
E-mail: s_yuhua@163.com
[b] State Key Laboratory of Coordination Chemistry, Nanjing University,
Nanjing 210093, P. R. China
Supporting information for this article is available on the WWW under http://www.eurjic.org or from the author.

Compared with other Keggin ions, TSA anions, $[SiW_{12}O_{40}]^{4-}$, have a wider pH range, which is up to about 5.5 (whereas $[PW_{12}O_{40}]^{3-}$ is at about 1.0)[24] and a high photocatalytic redox ability.[25] TSA is thus the preferred ion for the synthesis of CuI.

Results and Discussion

Crystal Structure and Morphology

The phase purity of the prepared products was determined by XRD. Figure 1 shows the XRD patterns of the prepared diamond-shaped CuI (a), CuI platelets obtained with I^- (b) and I_2 (c) as the iodine source. It is well known that CuI has three phases: the low-temperature γ phase, the high-temperature fluorite-type α phase and an intermediate β phase. The γ phase CuI has a zinc blende structure and the α phase CuI has a random distribution of copper ions over all tetrahedral sites.[26] Part A of Figure 1 shows that all samples can be indexed with the cubic zinc blende structure of CuI with cell parameters a = Å which is consistent with the literature values (JCPDS card number 83-1137) and no other impurity peaks were detected. The corresponding intact (111) peaks are shown in Figure 1 (B) and display the unusually strong diffraction peak intensity of the (111) plane, implying a preferential growth orientation of CuI crystals along the <100> direction. However, the relative intensity of the peaks corresponding to the values of the (111)/(220) and (311)/(222) planes vary from the above-mentioned CuI products [(a): 5.08 and 1.11; (b): 5.54 and 1.21; (c): 2.21 and 1.80], indicating the possible special tropism of the products.

The morphologies and sizes of the products were examined by TEM and SEM. Figures 2 (A, B) show typical SEM and TEM images of the diamond-shaped CuI nanocrystals. It can seen that the crystals have an average length of about 90 nm and excellent dispersibility. The representative TEM image of a diamond-shaped CuI unit (Figure 2, C) clearly shows that the particle has a height of about 90 nm, a base width of about 50 nm and a waist width of about 70 nm. The corresponding select area electron diffraction pattern (SAED) obtained by aligning the electron beam perpendicular to the planar surface shows sixfold rotational symmetry for the diffraction spots (Figure 2, D) which indicates the single-crystalline nature and the preferred {111} plane orientation of the diamond-shaped nanocrystal. Energy-dispersive X-ray (EDX) analysis (Figure 2, E) suggests that the elemental ratio of the Cu/I is 1:1.11 which is near the standard stoichiometric composition. The Au signal (2.2 eV) observed in the spectrum is due to Au sputtering,

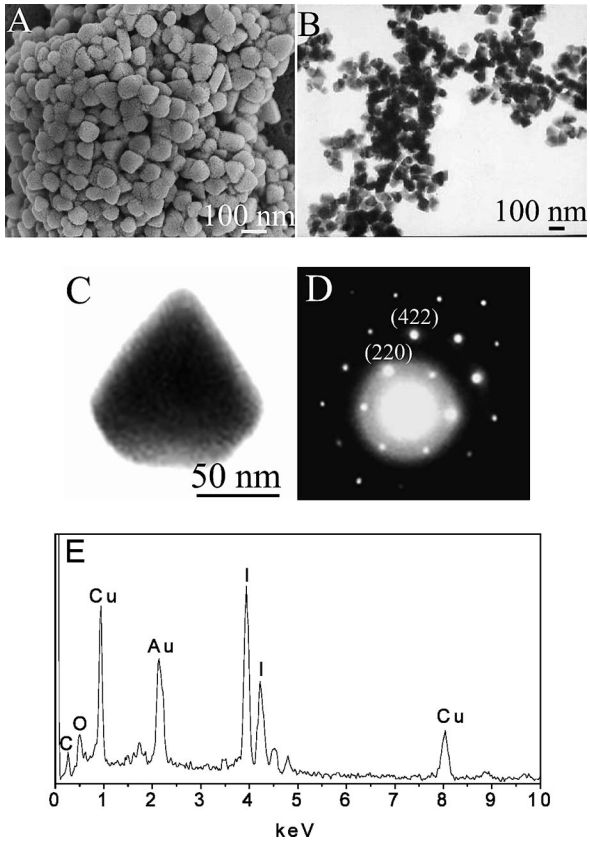

Figure 2. (A–C) SEM and TEM images of the prepared diamond-shaped CuI. (D) SAED pattern taken from the crystal of part C. (E) The corresponding EDX spectrum taken on the crystals shown in part A.

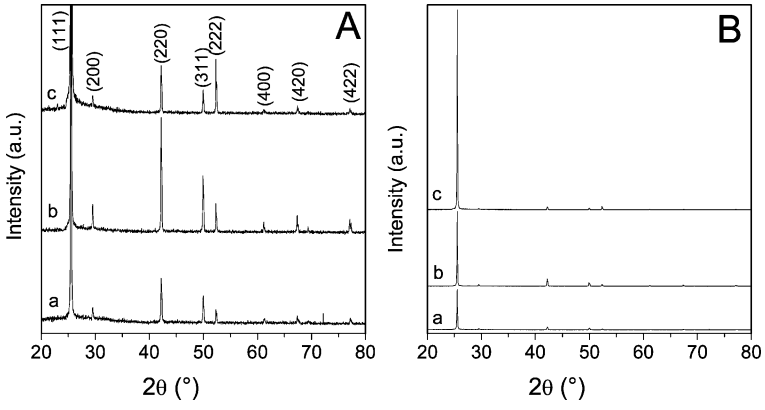

Figure 1. XRD patterns of the prepared diamond-shaped CuI (a), platelets obtained with I^- (b) and I_2 (c) as the iodine source, respectively. (A) The peaks of (111) are truncated. (B) The intact peaks of (111) are shown.

the Au being used for improving the surface conductivity of the SEM sample.

The surface composition of synthesised diamond-shaped CuI nanocrystals was further analyzed by XPS. The typical XPS results are shown in Figure 3, including the survey spectrum (A), Cu 2p (B) and I 3d (C). The strong peaks at 932.0 eV for Cu and at 619.2 eV for I may be observed which is in good agreement with the literature data for CuI material.[27] The weak peaks of O and C might come from H_2O, O_2 and CO_2 adsorbed on the surface of CuI nanocrystals in air.

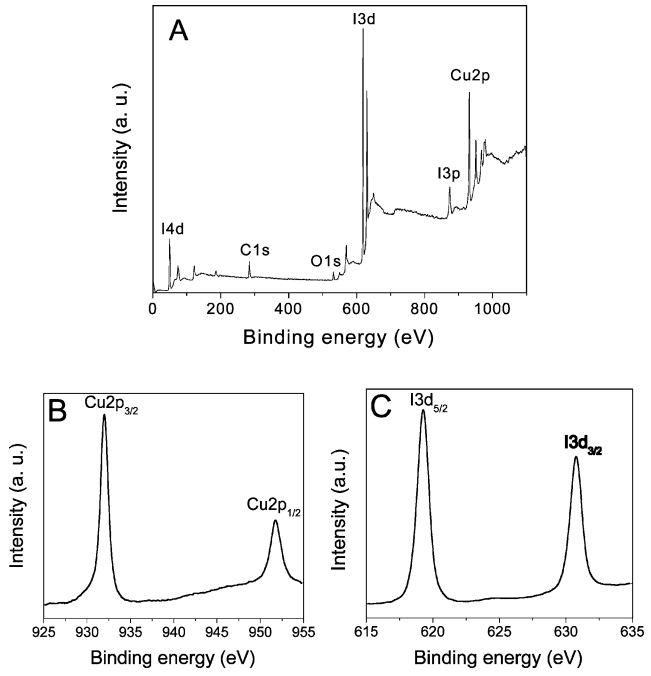

Figure 3. XPS core level spectra taken for the diamond-shaped CuI crystal: (A) survey, (B) Cu2p and (C) I3d.

Figure 4 shows the typical SEM and TEM images of the prepared CuI platelets obtained with I^- as the iodine source. The general overview SEM and TEM images (Figure 4, A and C) show that the platelets have hexagonal or truncated triangular (or asymmetric hexagonal) shapes with edge lengths of 100–500 nm. The side view SEM image (Figure 4, B) reveals that the thickness of the platelet is about 90 nm. The corresponding SAED pattern (Figure 4, D) displays the single-crystalline nature and preferential {111} plane orientation. Three representative platelets were studied by using SEM images. A truncated trigonal platelet with an edge length of 350 nm, an equilateral hexagon with an edge length of 250 nm and an asymmetric hexagon with the edge length of 100–300 nm are respectively exhibited in Figure 4 (E–G). The thickness of all the above mentioned platelets is estimated to be in the range of 60–90 nm from the SEM images. To further view the shape of the above three representative platelets, they were also examined by using TEM images which are shown in Figure S1 (parts A–C) of the Supporting Information.

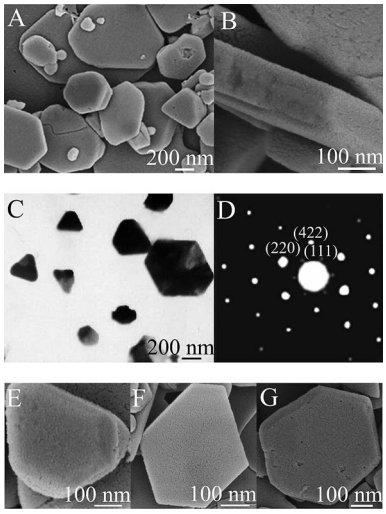

Figure 4. The general view (A) SEM and (C) TEM images of the prepared CuI platelets obtained with I^- as the iodine source. (B) The side view SEM image of a platelet. (D) SAED pattern taken from a single platelet. (E–G) SEM images of three representative platelets.

Figure 5 shows the SEM image of the prepared CuI sample obtained with molecular iodine (I_2) as the iodine source. Again, a mixture of hexagonal and truncated triangular platelets can be observed. Compared with Figure 4 (A), the morphology of this sample has no significant difference which can be attributed to the fact that I_2 is reduced to I^- first.

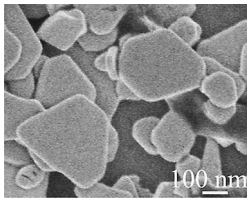

Figure 5. SEM image of the prepared CuI platelets obtained with I_2 as the iodine source.

Optical Properties

Figure 6 (A) shows the UV/Vis absorption spectra recorded on the UV-irradiated TSA solution at different time intervals. Prior to UV irradiation, no absorption in the visible region could be observed. Two absorption bands at 480 and 760 nm that are characteristic absorptions of reduced TSA ions can be found after irradiation.[16] Their intensities increase with time, suggesting that more TSA is becoming reduced. After about 3 h, there is no obvious change in the absorption bands indicating that all the TSA has been completely reduced. The colours of the solution at several typical stages are shown in the inset of Figure 6 (A). Under UV radiation, the colour of the solution gradually changed from colourless to blue and, finally, to blue-black.

Figure 6 (B) shows the UV/Vis absorption spectra of diamond-shaped CuI recorded from the stock solution (curve

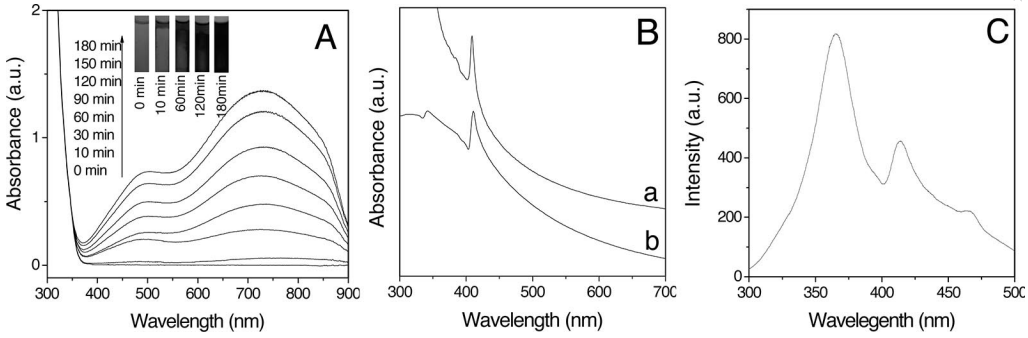

Figure 6. (A) UV/Vis absorption spectra of irradiated TSA solutions at various times. Inset shows the colour of irradiated TSA solutions at several typical stages. (B) UV/Vis absorption spectra of diamond-shaped CuI measured from the stock solution (a) and the prepared CuI sample redispersed in distilled water (b). (C) Room temperature PL spectrum of the prepared CuI sample.

a) and the prepared sample redispersed in distilled water (curve b). After adding Cu^+ and I^-, the absorption bands of reduced TSA disappeared which indicates that all the reduced TSA ions are oxidised by Cu^{2+}. On the other hand, the appearance of the absorption peaks at 410 nm is indicative of the formation of CuI. The prepared CuI sample exhibits two absorption peaks at 339 and 410 nm. The hump at 339 nm can be attributed to the excitation of electrons from sub bands in the valance to the conduction band whereas the stronger peak at 410 nm originates from the excitation of electrons from the valance band to the conduction band.[11]

Figure 6 (C) shows the room temperature PL spectrum of the prepared diamond-shaped CuI sample, as measured with an excitation wavelength of 276 nm. It displays an intensive emission at 365 nm, accompanied by a secondary feature present at 414 nm and an additional weak emission at 466 nm. The observed emission band at 414 nm is due to the iodine-related surface trap recombination[20,28] which mainly exists in the (111) CuI crystal. It is known that copper has a small ionic radius of 0.074 nm and iodide has a huge ionic radius of 0.206 nm causing iodide to be tightly squeezed into the tightly packed (111) face during growth. It can lead to a high probability of an iodide vacancy formation.[29] Such surface defect bands are the most common in previous reports.[11,30] However, from the viewpoint of crystal growth design for yielding a perfect crystal structure of CuI, a strong emission of the defect band is not desirable due to the presence of lots of crystal defects. As for the effect of surface iodide vacancies upon composition of the CuI crystal, and although lots of iodide vacancies exist on the crystal surface, CuI crystals always contains a stoichiometric excess of iodine in the bulk[29,31] which causes stoichiometric or over-stoichiometric amounts of iodine in the CuI crystal. The emission bands at 365 and 466 nm for CuI have not been reported previously, we speculate that the former can be assigned to recombination from the excitonic state in the crystallite interior and the latter can be attributed to the defect of the other crystal face. The PL quantum yield (QY) calculated relative to rhodamine B in ethanol as a standard sample is about 1.8%. The low QY value is probably due to the presence of surface traps and the reduced quantum confinement of the large sizes of the crystals.

Figure 7 (A) shows the time-dependent UV/Vis spectra for the CuI platelets obtained with I^- as the iodine source under UV irradiation. The characteristic absorption of CuI (410 nm) can be observed after UV irradiation for about 10 min and its strength promptly increases with extended irradiation indicating that more CuI is produced. At the same time, the clear colourless solution changes to a white colloidal suspension. After about 120 min, the intensity of the absorption peaks of CuI no longer increases and a weak absorption band at 700 nm can be detected. This absorp-

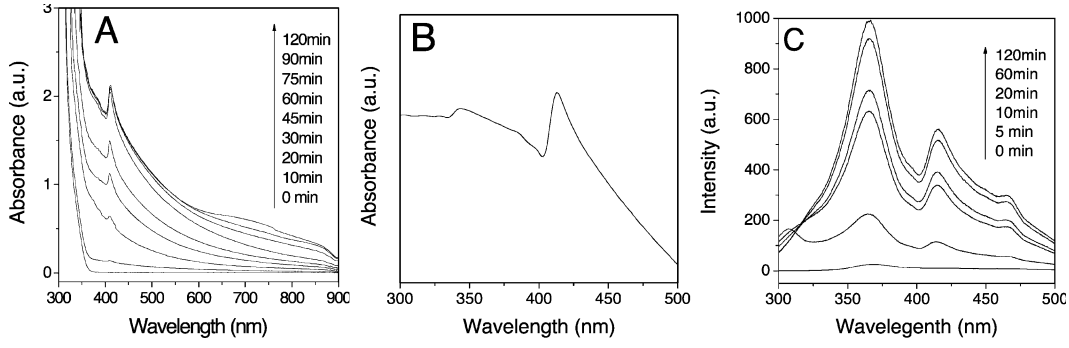

Figure 7. (A) Time-dependent UV/Vis absorption spectra for CuI platelets obtained with I^- as the iodine source. (B) UV/Vis absorption spectrum of the prepared CuI platelets. (C) The corresponding time-dependent room temperature PL spectra of generated CuI platelets.

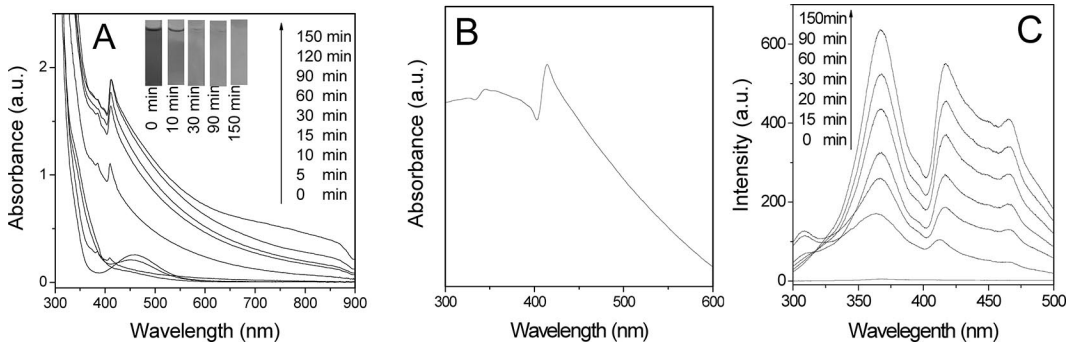

Figure 8. (A) Time-dependent UV/Vis absorption spectra for CuI platelets obtained with I_2 as the iodine source and the inset shows the colour of irradiated solution mixtures at several typical stages. (B) UV/Vis absorption spectrum of the prepared CuI platelets. (C) The corresponding time-dependent room temperature PL spectra of generated CuI platelets.

tion band arises due to the formation of reduced TSA, indicating that all Cu^{2+} ions in the solution have been completely turned to Cu^{+} ions. Figure 7 (B) shows the UV/Vis absorption spectrum of the prepared CuI sample redispersed in distilled water which is similar to curve b of Figure 6 (B). The generation of CuI platelets can also be followed by the time-dependent room temperature PL spectra (Figure 7, C), measured with an excitation wavelength of 276 nm. Under UV irradiation for about 10 min, the emissions at 365, 414 and 466 nm can be synchronously observed and their intensity increases with increasing time. The greatest change appeared in the period after 10–20 min, indicating that most CuI product was produced in this stage and this is consistent with the time-dependent UV/Vis spectra. The maximum reaction rate does not occur at the first 10 min possibly due to induction and energy accumulation during this period. The QY of this sample is about 1.5% which is lower than that for the diamond-shaped CuI.

The generation of CuI platelets using I_2 as iodine source was also studied by UV/Vis absorption and PL spectroscopy. The absorption band at 455 nm observed in the first 15 min from the time-dependent UV/Vis spectra (Figure 8, A) can be ascribed to molecular iodine. The absorption of CuI is only found after the disappearance of the absorption band of I_2. Hence the synthesis needs a much longer time (about 150 min) than that using I^- as the iodine source, something which is also confirmed by the time-dependent PL spectra (Figure 8, C). The reaction could be easily observed by the solution colour change from yellow to light white, as shown in the inset A of Figure 8. Part B of Figure 8 shows that the prepared CuI platelets also have a similar absorption band with the above mentioned samples (see part B, curve b in Figure 6 and part B of Figure 7). However, the PL emission peak at 414 nm is more intense than that in Figure 6 (C) and Figure 7 (C) which may be due to the more highly oriented CuI (111) grains of the present sample. Such a result has been substantiated by XRD patterns. The intense emission at 414 nm also means an imperfect crystal structure for the present sample.

Electrical Properties

To study the electric properties of the prepared CuI nanocrystals, real-time current measurements were taken and are shown in Figure 9. Clearly, the diamond-shaped CuI nanocrystals (curve a) have a higher current intensity than CuI platelets synthesised with I^- as the iodine source (curve b) suggesting the lower resistance of diamond-shaped CuI particles and this may be due to small size effects and surface effects. The affinitive relationship of the size and the property indicates potential for the design and preparation of special building blocks in nanoscale electronic device fabrications.

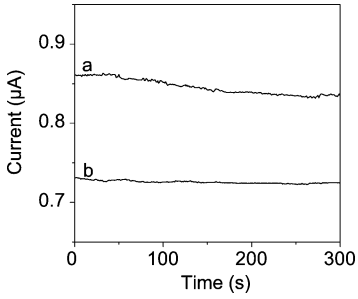

Figure 9. Real-time detection of the current for prepared (a) diamond-shaped CuI and (b) platelets obtained with I^- as the iodine source.

Possible Growth Mechanism of Diamond-Shaped and Platelet-Shaped CuI Crystals

The formation of CuI crystals in the presence of TSA occurs by a photochemical reaction based on the equations below.

Reactions (1) and (2) provide an overall account of the photocatalytic oxidation of the organic and the concomitant formation of reduced TSA ($[SiW_{12}O_{40}]^{5-}$). Details, i.e. formation of radicals involved in the process etc., have been reported elsewhere.[32] The photochemically reduced TSA species can, in turn, deliver the electrons to a great variety

of chemical species such as metal ions, molecular oxygen and molecular iodine etc. Since the redox properties of Keggin ions can be widely and precisely varied, depending on the nature of the polyanions, manipulation of the efficiency of the process can be achieved by selecting Keggin ions with appropriate redox potentials.[25] Based on the redox potentials, TSA ions (E^0 $SiW_{12}O_{40}^{4-/5-}$ = 0.057 V vs. NHE) are more efficient in reducing metal ions than the other Keggin ions such as $[PW_{12}O_{40}]^{3-}$ (E^0 $PW_{12}O_{40}^{3-/4-}$ = 0.221 V vs. NHE). In the present study, both I_2 and Cu^{2+} ions can be reduced by photoreduced TSA ions as depicted in Equations (3) and (4). When I_2 served as the iodine source, they can be firstly reduced to I^- ions [E^0 (I^0/I^-) = 0.535 V vs. NHE]. As for the reduction of Cu^{2+}, generally, it is a two-step process in which Cu^+ is initially formed, the latter being then further reduced to zero-valent copper [E^0 (Cu^{2+}/Cu^0) = 0.337 V, E^0 (Cu^{2+}/Cu^+) = 0.153 V, E^0 (Cu^+/Cu^0) = 0.521 V vs. NHE]. However, the Cu^+ is very unstable in aqueous solution. Here, the formation of Cu^+ can be ascribed to the poor solubility of CuI, as indicated in Equations (5) and (6), and the moderate reducing ability of $[SiW_{12}O_{40}]^{5-}$ ions.

$$[SiW_{12}O_{40}]^{4-} + h\nu \leftrightarrow [SiW_{12}O_{40}]^{4-}* \quad (1)$$

$$[SiW_{12}O_{40}]^{4-}* + CH_3CH_2OH \rightarrow [SiW_{12}O_{40}]^{5-} + CH_3CHO \quad (2)$$

$$[SiW_{12}O_{40}]^{5-} + I_2 = 2I^- + [SiW_{12}O_{40}]^{4-} \quad (3)$$

$$[SiW_{12}O_{40}]^{5-} + Cu^{2+} = Cu^+ + [SiW_{12}O_{40}]^{4-} \quad (4)$$

$$I^- + Cu^+ = CuI \quad (5)$$

$$I^- + Cu^{2+} + e = CuI \quad (6)$$

To further study the important function of TSA in the reduction of Cu^{2+} to Cu^+, UV irradiation was substituted by the addition of solutions of the reducing agent $NaBH_4$ in the presence and absence of TSA, described in the "control experiment" of the synthetic procedures part of the experimental section (vide infra). Part A of Figure 10 shows the UV/Vis absorption spectra of the mixture containing TSA before (curve a) and after (curves b–g) the addition of $NaBH_4$. After addition of $NaBH_4$, the characteristic absorption of CuI can be observed directly and its intensity increases in the first 2 h indicating that more CuI is being produced. Upon further ageing for 24 h, single crystal CuI platelets with the trigonal shape are obtained (Figure S2 of Supporting Information). It is worth pointing out that no plasmon resonance of elemental Cu appeared in this process. When the reduction of Cu^{2+} is performed in the absence of TSA, an absorption band centred at 565 nm, which corresponds to the plasmon absorption band of Cu, can be instantly detected after addition of the $NaBH_4$ solution (part B of Figure 10, curve b). When the resultant deep red Cu colloidal solution is exposed to air, Cu can be oxidised by oxygen in the air to Cu_2O (Figure 10, B, curves c–f). After 24 h, single crystal Cu_2O platelets are obtained (Figure S3 of Supporting Information). Under these conditions, Cu^{2+} ions are thoroughly reduced to elemental copper and no characteristic absorption of CuI can be observed. All of the evidence indicates that the formation of Cu^+ not only depends on the precipitation of CuI but also on a suitable reducing agent of reduced TSA. In the presence of TSA, TSA ions rather than Cu^{2+} ions are firstly reduced by $NaBH_4$. The reduced TSA ions then reduce Cu^{2+} to Cu^+ which is promptly precipitated by I^- ions. All the above reactions can be generalised as in equation 6 [E^0 (Cu^{2+}/Cu^+) = 0.86 V vs. NHE].

In the cubic zinc blende structure CuI crystal, each Cu^+ ion is tetrahedrally surrounded by four I^- ions. Figure 11 (left) indicates that I^- and Cu^{2+} ions are tetrahedrally coordinated by the respective counterions and the CuI crystal is composed of many coordinated ICu_4 groups.[33] The growth

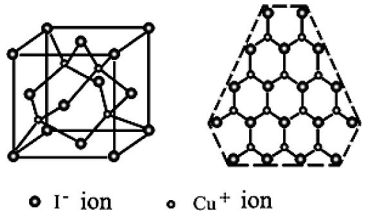

Figure 11. Schematic diagram of the cubic zinc blende structure cell (left) and the growth mechanism illustration of CuI crystal along the direction perpendicular to {111} plane (right).

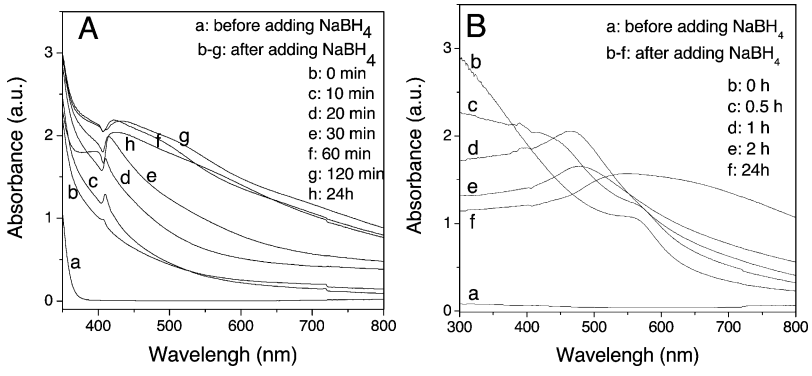

Figure 10. UV/Vis absorption spectra of the reaction mixtures in (A) presence and (B) absence of TSA measured before and after addition of $NaBH_4$.

of highly oriented (111) γ-CuI is shown in Figure 11 (right) which is cut thought the fcc unit cell perpendicular to (111). The general growth process of CuI crystals has been proposed by W. J. Li et al.[6] They assumed that the growth of a γ-CuI crystal consists of the complexation of I^- ions to Cu^+ ion to form CuI_4 groups and the complexation of Cu^+ ions to I^- ions to form ICu_4 groups at the interface, and that the two kinds of coordination processes proceed alternately at the interface.

In our study, when Cu^{2+} and I^- are synchronously added to the reduced TSA solution, Cu^{2+} ions are reduced instantly, resulting in the supersaturation of Cu^+ and I^- which leads to the homogeneous nucleation of γ-CuI. Generally, homogeneous nucleation occurs in the absence of a solid interface by combining solute molecules to produce nuclei. Homogeneous nucleation happens due to the driving force of the thermodynamics because the supersaturated solution is not energetically stable.[34] Homogeneous nucleation of tetrahedral nuclei with the zinc blende crystal structure is favoured by the fact that these tetrahedra expose only close-packed {111} facets and that stoichiometric and complete tetrahedra can form for a large number of closely spaced cluster sizes.[35] The formation of uniform nanosized diamond-shaped CuI crystals is determined by the high ratio of the growth rate in the <100> direction to that in the <111> direction and mass nucleation in the supersaturation solution which is depicted by route A in Figure 12.

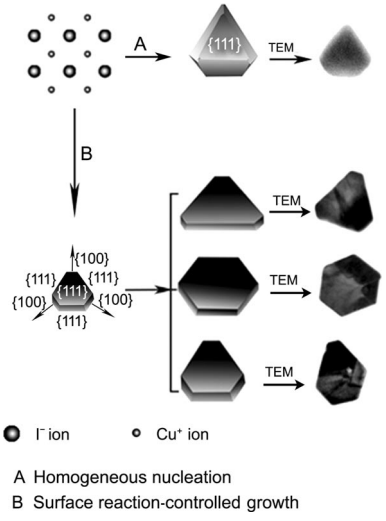

Figure 12. Schematic illustration of the growth paths leading to diamond-shaped and platelet-shaped CuI crystals.

When the nucleation and growth of CuI crystals is performed under UV irradiation, surface reaction-controlled growth is dominant. Generally, the reaction-controlled growth usually leads to a broad size distribution.[36] As we known, {111} facets of many crystals with the cubic zinc blende structure have the lowest energy.[37,38] Moreover because the {111} facet is polar and tends to adopt the polar solute and solvent in the growth process,[29] both TSA ion and I^- can be specific for binding to {111} facets of the CuI crystal which further lowers the energy of these facets. The presence of low energy facets drives the growth of nuclei in a 2D manner to produce a platelet morphology with confined {111} planes.[39] The combination of Cu^+ ions and I^- ions is continuously taken at the interface of the side faces which results in an epitaxial growth of hexagonal platelets. The flat top and bottom facets of these hexagonal plates should be bound by {111} planes and the six side faces by three {111} and three {100} planes, as shown by the geometrical model in route B of Figure 12. The formation of hexagonal and truncated triangular (or asymmetric hexagonal) shapes is due to different growth rates on the three {100} planes.

Conclusions

In summary, we have successfully synthesised single-crystalline diamond-shaped γ-CuI and platelets by a photochemically reduced TSA route at room temperature. Two iodine sources of I^- and I_2 were used for the formation of platelets and the growth processes have been monitored by UV/Vis absorption and by room temperature PL spectra. The emission at 365 nm is observed initially and the emission at 414 nm is related to the surface defect of the {111} planes. The real-time electric current measurement shows that the current intensity of diamond-shaped CuI nanocrystals is higher than that of the platelets which means a better conductibility of the former for potential applications in superionic conductor, solid-state solar cells etc. The formation of diamond-shaped CuI nanocrystals is possibly followed a homogeneous nucleation mechanism and the formation of the platelets can be explained by a tropism growth theory.

Experimental Section

Materials: All reagents used in this work, including 12-tungstosilicate (TSA), copper sulfate ($CuSO_4$), potassium iodide (KI), iodine (I_2), ethanol and sodium borohydride ($NaBH_4$) were analytical grade and used as received without further treatment. Double-distilled water was used in all experiments.

Synthetic Procedures

Synthesis of Single-Crystalline Diamond-Shaped CuI Nanostructures: First, ethanol (2 mL) was added to a 4 mM TSA deaerated solution (25 mL) and the mixture was irradiated with UV light (Pyrex filter, >280 nm, 450-W Hanovia medium-pressure lamp) for 3 h. After irradiation, the colour of the solution changed from colourless to blue-black, indicating the formation of reduced TSA ($[SiW_{12}O_{40}]^{5-}$). The reaction process was followed by UV/Vis absorption spectroscopy. Next, to the photochemically reduced TSA solution were simultaneously added 4 mM $CuSO_4$ (2.5 mL) and 0.8 mM KI (12.5 mL) deaerated solutions under nitrogen and with stirring. The blue-black solution turned to colourless immediately and then to a white colloidal suspension suggesting the formation of CuI nanocrystals. Finally, the white product was separated out by centrifuging and washed several times with distilled water and absolute ethanol and the final product was dried in a vacuum at 80 °C for 5 h for further characterisation.

Synthesis of Single-Crystalline CuI Platelets: For this synthesis, KI and I_2 were used as iodine sources, respectively. In a typical pro-

cedure, ethanol (5 mL) was added to a deaerated solution mixture (50 mL) which consisted of TSA (2 mM), $CuSO_4$ (1 mM) and KI (2 mM). The final solution mixture was then irradiated with UV light. After 10 min, the solution slowly changed from clear to a white colloidal suspension, indicating the formation of CuI nanocrystals. The temporal evolution of CuI growth was monitored by UV/Vis absorption and PL spectroscopy. After irradiation for 2 h, the resultant product was thoroughly washed and dried as in the above-mentioned procedure. Following this, the other CuI platelets were prepared with I_2 as the iodine source but, in contrast, using I_2 (5 mL, 10 mM) in ethanol which was added to a deaerated solution (50 mL) containing TSA (2 mM) and $CuSO_4$ (1 mM). The solution mixture was UV-irradiated for 2.5 h and the precipitate was also collected for further characterisation.

Control Experiment: To further study the effect of TSA on the formation of CuI, the synthesis was carried out by substituting UV irradiation with the addition of $NaBH_4$ in the presence or absence of TSA. Briefly, to a solution (25 mL) containing TSA (2 mM), $CuSO_4$ (2 mM) and KI (4 mM) and to another solution (25 mL) containing $CuSO_4$ (2 mM) and KI (4 mM) was added $NaBH_4$ (25 mL, 10 mM). After magnetic stirring for 10 min, both reactions were then exposed to air for 24 h. The above processes were followed by using a UV/Vis absorption spectrometer and all the products were collected for further characterisation.

Measurement: The crystal structure was characterised by X-ray diffraction (XRD) on a MAP-18-AHF wide angle goniometer with Cu-K_α radiation (λ = 1.5418 Å). X-ray photoelectron spectroscopy (XPS) was obtained on an ESCALab MKII X-ray photoelectron spectrometer, using Mg-K_α radiation as the excitation source. TEM images and SAED patterns were taken at an accelerating voltage of 100 kV on a JEM model 100SX instrument. HE-SEM measurements were performed on a JEOL-6700F instrument equipped with EDX capabilities. UV/Vis absorption spectra were taken on a JASCO V-570 spectrophotometer with a 1 cm quartz cell. Photoluminescence (PL) measurements were carried out at room temperature on a luminescence spectrometer (Perkin–Elmer, LS50B) with a resolution of 1.0 nm using 275 nm as the excitation wavelength. PL quantum yields were measured using a rhodamine B standard (QY = 0.696) in ethanol. For current measurements, 50 mg of CuI samples were ultrasonically treated and dispersed on quartz substrates with a length of 2 cm and width of 1 cm. The measurements were taken using a picoammeter/voltage source (Keithley 6487) in the range 0–500 V, the dc current sensitivity of the system is in the range 10^{-14} A. A bias voltage was set at V = 0.1 V in all of the experiments.

Supporting Information (see also the footnote on the first page of this article): TEM images of three representative platelets obtained with I^- as the iodine source, TEM images and SAED pattern of CuI triangle platelets obtained with $NaBH_4$ as reducing agent and TEM images and SAED pattern of the prepared Cu_2O triangle platelets.

Acknowledgments

This work is supported by the National Science Foundation of China (Grants 20871001, 20671001 and 20731001), the Major Program of Anhui Provincial Education Department (Grant ZD2007004-1), the Research Fund for the Doctoral Program of Higher Education of China (20070357002) and the Foundation of Key Laboratory of Environment-Friendly Polymer Materials and Functional Material of Inorganic Chemistry of Anhui Province.

[1] Z. Zhang, S. H. Lee, J. J. Vittal, W. S. Chin, *J. Phys. Chem. B* **2006**, *110*, 6649–6654.
[2] M. Ethayaraja, C. Ravikumar, D. Muthukumaran, K. Dutta, R. Bandyopadhyaya, *J. Phys. Chem. C* **2007**, *111*, 3246–3252.
[3] T. H. Wei, C. W. Chen, L. C. Hwang, P. L. Tu, T. C. Wen, *J. Lumin.* **2008**, *128*, 161–165.
[4] Y. Yang, X. Li, B. Zhao, H. Chen, X. Bao, *Chem. Phys. Lett.* **2004**, *387*, 400–404.
[5] C. Chen, P. G. Dormer, *J. Org. Chem.* **2005**, *70*, 6964–6967.
[6] W. J. Li, E. W. Shi, *Cryst. Res. Technol.* **2002**, *37*, 1041–1048.
[7] L. P. Zhang, F. Guo, X. Z. Liu, *Mater. Res. Bull.* **2006**, *41*, 905–908.
[8] P. Gao, M. Gu, X. L. Liu, *Cryst. Res. Technol.* **2008**, *43*, 496–501.
[9] X. Li, M. Wan, *Cryst. Growth Des.* **2006**, *6*, 2661–2666.
[10] C. H. B. Ng, W. Y. Fan, *J. Phys. Chem. C* **2007**, *111*, 9166–9171.
[11] Y. Xu, D. Chen, X. Jiao, L. Ba, *J. Phys. Chem. C* **2007**, *111*, 6–9.
[12] M. T. Pope, A. Müller, *Angew. Chem. Int. Ed. Engl.* **1991**, *30*, 34–48.
[13] T. Okuhara, N. Mizuno, M. Misono, *Adv. Catal.* **1996**, *41*, 113–252.
[14] L. Hill, D. A. Bouchard, M. Kadkhodayan, M. M. Williamson, J. A. Schmidt, E. F. Hilinski, *J. Am. Chem. Soc.* **1988**, *110*, 5471–5479.
[15] C. M. Teague, X. Li, M. E. Biggin, L. Lee, J. Kim, A. A. Gewirth, *J. Phys. Chem. B* **2004**, *108*, 1974–1985.
[16] A. Troupis, A. Hiskia, E. Papaconstantinou, *Angew. Chem. Int. Ed.* **2002**, *41*, 1911–1914.
[17] A. Troupis, A. Hiskia, E. Papaconstantinou, *Environ. Sci. Technol.* **2002**, *36*, 5355–5362.
[18] S. Mandal, P. R. Selvakannan, R. Pasricha, M. Sastry, *J. Am. Chem. Soc.* **2003**, *125*, 8440–8441.
[19] S. Mandal, D. Rautaray, M. Sastry, *J. Mater. Chem.* **2003**, *13*, 3002–3005.
[20] S. Mandal, A. Das, R. Srivastava, M. Sastry, *Langmuir* **2005**, *21*, 2408–2413.
[21] L. B. Yang, Y. H. Shen, A. J. Xie, J. J. Liang, *Eur. J. Inorg. Chem.* **2007**, *28*, 4438–4444.
[22] L. B. Yang, Y. H. Shen, A. J. Xie, J. J. Liang, S. K. Li, Q. F. Zhang, *Eur. J. Inorg. Chem.* **2007**, *8*, 1128–1134.
[23] L. B. Yang, Y. H. Shen, A. J. Xie, B. C. Zhang, *J. Phys. Chem. C* **2007**, *111*, 5300–5308.
[24] V. Kogan, Z. Izenshtat, R. Neumann, *Angew. Chem. Int. Ed.* **1999**, *38*, 3331–3334.
[25] A. Troupis, E. Gkika, A. Hiskia, E. Papaconstantinou, *C. R. Chim.* **2006**, *9*, 851–857.
[26] M. Yashima, Q. Xu, A. Yoshias, S. Wada, *J. Mater. Chem.* **2006**, *16*, 4393–4396.
[27] J. F. Moulder, W. F. Stickle, P. E. Sobol, K. D. Bomben, in *Handbook of X-ray Photoelectron Spectroscopy* (Eds.: J. Chastain, R. C. King), Physical Electronics, Inc., Eden Prairie, Minnesota, **1995**.
[28] V. P. S. Perera, K. Tennakone, *Sol. Energy Mater. Sol. Cells* **2003**, *79*, 249–255.
[29] Z. Zheng, A. Liu, S. Wang, B. Huang, K. W. Wong, X. Zhang, S. K. Harkb, W. M. Lau, *J. Mater. Chem.* **2008**, *18*, 852–854.
[30] Y. Zhou, M. Lü, G. Zhou, S. Wang, S. Wang, *Mater. Lett.* **2006**, *60*, 2184–2186.
[31] V. P. S. Perera, K. Tennakone, *Sol. Energy Mater. Sol. Cells* **2003**, *79*, 249–255.
[32] A. Troupis, E. Gkika, T. Triantis, A. Hiskia, E. Papaconstantinou, *J. Photochem. Photobiol. A: Chem.* **2007**, *188*, 272–278.
[33] N. T. M. Hai, S. Huemann, R. Hunger, W. Jaegermann, K. Wandelt, P. Broekmann, *J. Phys. Chem. C* **2007**, *111*, 14768–14781.
[34] C. Burda, X. Chen, R. Narayanan, M. A. El-Sayed, *Chem. Rev.* **2005**, *105*, 1025–1102.

[35] K. T. Yong, Y. Sahoo, M. T. Swihart, P. N. Prasad, *J. Phys. Chem. C* **2007**, *111*, 2447–2458.
[36] X. G. Peng, J. Wickham, A. P. Alivisatos, *J. Am. Chem. Soc.* **1998**, *120*, 5343–5344.
[37] J. A. Sioss, C. D. Keating, *Nano Lett.* **2005**, *5*, 1779–1783.
[38] C. C. Li, W. P. Cai, B. Q. Cao, F. Q. Sun, Y. Li, C. X. Kan, L. D. Zhang, *Adv. Funct. Mater.* **2006**, *16*, 83–90.
[39] C. H. B. Ng, W. Y. Fan, *J. Phys. Chem. B* **2006**, *110*, 20801–20807.

Received: October 1, 2008
Published Online: February 18, 2009

